NANO LETTERS

2007
Vol. 7, No. 3
738−744

# Mapping Local Photocurrents in Polymer/Fullerene Solar Cells with Photoconductive Atomic Force Microscopy

**David C. Coffey, Obadiah G. Reid, Deanna B. Rodovsky, Glenn P. Bartholomew, and David S. Ginger***

*University of Washington, Department of Chemistry, Box 351700, Seattle, Washington 98195-1700*

*Received December 19, 2006; Revised Manuscript Received January 24, 2007*

**ABSTRACT**

**The performance of organic solar cells is highly dependent on film morphology. However, directly correlating local film structures with device performance remains challenging. We demonstrate that photoconductive atomic force microscopy (pcAFM) can be used to map local photocurrents with 20 nm resolution in donor/acceptor blend solar cells of the conjugated polymer poly[2-methoxy-5-(3′,7′-dimethyloctyl-oxy)-1,4-phenylene vinylene] (MDMO-PPV) with the fullerene (6,6)-phenyl-$C_{61}$-butyric acid methyl ester (PCBM) spin-coated from various solvents. We present photocurrent maps under short-circuit conditions (zero applied bias) as well as under various applied voltages. We find significant variation in the short-circuit current between regions that appear identical in AFM topography. These variations occur from one domain to another as well as on larger length scales incorporating multiple domains. These results suggest that the performance of polymer–fullerene blends can still be improved through better control of morphology.**

Conjugated polymers, small molecules, and colloidal semiconductor nanocrystals are promising materials for use in low-cost, solution-processable thin-film photovoltaic devices.[1−4] However, the power conversion efficiency of solar cells based on these materials is still below desired levels. In a typical solar cell made from a blend of organic semiconductors, light absorption creates strongly bound excitons that must be dissociated into free charges at a donor/acceptor interface.[5,6] These excitons can migrate ∼10 nm before they decay, while films ∼100 nm thick are required for efficient light absorption. This mismatch of length scales, sometimes referred to as the excitonic bottleneck, has led to many designs for nanostructured organic solar cells with large internal surface areas.[7,8] For many devices, donor and acceptor materials are processed from a common solvent into a phase-separated film.[9−11] By using different solvents and postprocessing conditions, one seeks to produce donor/acceptor interfaces throughout an optically thick film while retaining connected pathways of each material type to facilitate charge extraction. Practically, small changes in processing conditions can alter a blended film's morphology and induce dramatic and often unexpected variations in overall efficiency.[9−29] As a result, much progress in the field is currently based on trial-and-error optimization, and there is a great deal of interest in obtaining a microscopic understanding of how morphology impacts device performance.

Toward this end, various microscopies including transmission electron microscopy (TEM),[12−14] atomic force microscopy (AFM),[12−15] and scanning transmission X-ray microscopy (STXM)[15] have been used to study the morphology of nanostructured organic thin films. However, while such methods provide information about film structure, they cannot provide direct information about how the individual nanostructures evident in the micrographs contribute to device performance; this information must be inferred by correlating the microscopy with separate device measurements. To obtain more direct correlations between morphology and device performance, several groups have employed optical or electrical scanning-probe techniques to examine the composition-dependent optoelectronic properties of photovoltaic blends. Near-field scanning optical microscopy (NSOM) has been used to measure local fluorescence and photocurrents with ∼200 nm resolution.[16−21] Scanning Kelvin probe microscopy (SKPM) has been used to measure local open-circuit voltages with ∼50−100 nm resolution, although trapped charge can complicate data analysis.[22,23] Recently, our group introduced time-resolved electrostatic force mi-

* Corresponding author. E-mail: ginger@chem.washington.edu. Telephone: (206)685-2331. Fax: (206)685-8665.

10.1021/nl062989e CCC: $37.00 
**Published on Web 02/13/2007**

croscopy (trEFM), a new method capable of measuring photoinduced charging rates with ~50−100 nm resolution, and we showed that these rates can be used to map the local external quantum efficiency (EQE) of polyfluorene blends.[24] These results have underscored the need for further microscopic studies by finding that our intuitive picture of how local topographical features correlate with performance is not always accurate. Nevertheless, none of these techniques can yet image the optoelectronic properties of films with a resolution approaching the exciton diffusion length (~10 nm).

Herein, we describe a significant step in this direction: the use of photoconductive-AFM (pcAFM) to map photocurrent distributions in organic photovoltaic blends with ~20 nm resolution. While conductive-AFM (cAFM) has been widely used to measure the local electronic properties of organic films,[30−36] even of photovoltaic fullerene blends,[37] we are not aware of any reports describing the use of cAFM to image photocurrent distributions in organic thin films. We accomplish this by aligning a cAFM probe at the center of a diffraction-limited laser spot, which generates enough photocurrent signal to facilitate imaging at modest current levels (~1−10 pA at low intensity, or ~1 nA at high intensity). Not only does pcAFM achieve ~20 nm resolution when imaging photocurrents, but it also allows us to study the intensity dependence of the photocurrent over nearly 6 orders of magnitude in illumination intensity. As our test system, we apply this technique to the study of poly[2-methoxy-5-(3′,7′-dimethyloctyl-oxy)-1,4-phenylene vinylene]:(6,6)-phenyl-$C_{61}$-butyric acid methyl ester (MDMO-PPV:PCBM) blends, a system that has received considerable attention as a photovoltaic material.[11−15,22,29,37,38]

We performed pcAFM on the same films that we used to make standard, millimeter-sized photovoltaic cells. These devices were fabricated on indium tin oxide (ITO) coated glass substrates (TFD, Inc., Anaheim, CA) as follows. First, a 40 nm PEDOT:PSS (Baytron P VP Al 4083) layer was spin-coated and cured at 110 °C for 30 min. Second, an ~80 nm MDMO-PPV:PCBM active layer was deposited by spin-coating. PCBM was purchased from American Dye Source (Quebec, Canada), and MDMO-PPV, except where specifically noted, was synthesized in house (Supporting Information).[39] The MDMO-PPV:PCBM films were spin-coated from chlorobenzene, xylenes, or toluene to yield varying scales of phase separation. Forty nanometer thick aluminum top contacts were evaporated through a shadow mask to define active devices 1.5 $mm^2$ in area. Bulk device measurements were made in vacuum at 5 mB under an average monochromatic intensity of 10 W $m^{-2}$. Bulk device photocurrent action spectra and current−voltage characteristics were read using a digital source-measure unit (Keithley model 2400). EQEs were calculated by taking the ratio of the device photocurrent to the corrected photocurrent of a Si-photodiode with a calibrated spectral response. Further experimental details can be found in the Supporting Information.

Photoconductive-AFM was performed on the same samples used for bulk devices studies, in the areas between the aluminum electrodes. Figure 1a shows an experimental schematic. Samples were imaged with an atomic force microscope (Asylum Research, MFP-3D) in a nitrogen flow cell positioned above an inverted optical microscope. The AFM's feedback diode has a wavelength of 860 nm, far outside the absorption profile of either MDMO-PPV or PCBM. Voltages were applied between the ITO substrate and the conductive probe tips, and the current was recorded by the AFM's internal preamplifier (Asylum Research,

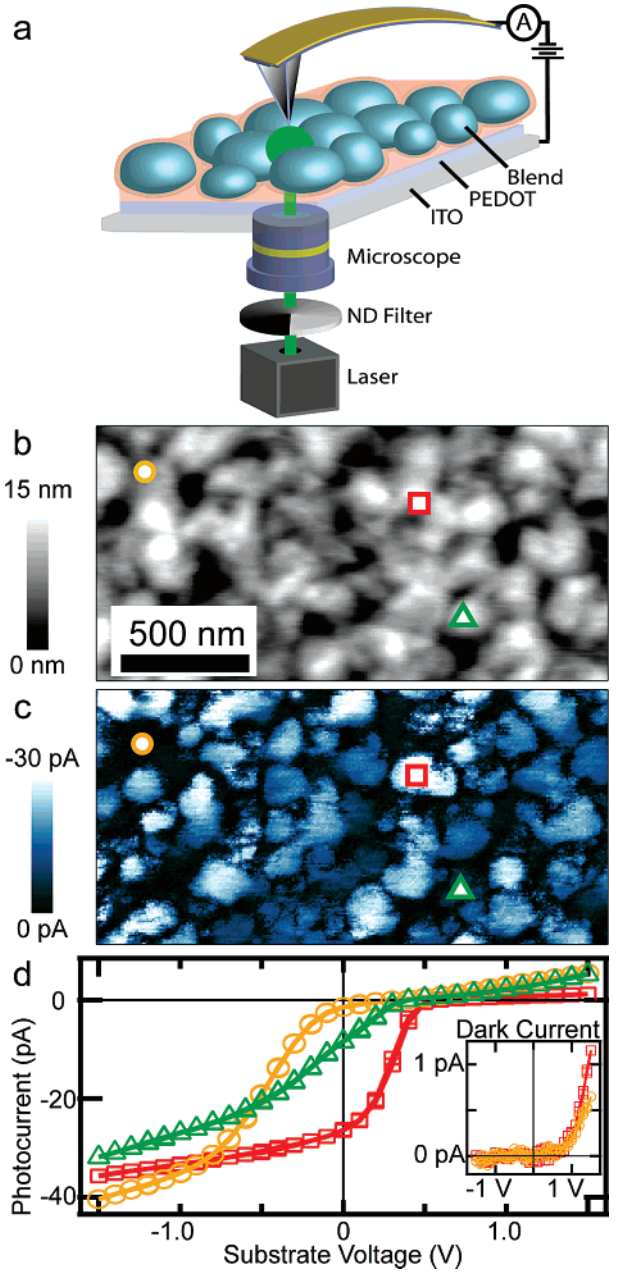


**Figure 1.** (a) Experimental schematic of a laser focused through a transparent electrode onto a photovoltaic blend film. Current is collected with a metal-coated AFM tip. (b) AFM height image of an MDMO-PPV:PCBM 20:80 film spin-coated from xylenes. (c) Photocurrent map measured with zero external bias and an illumination intensity of ~$10^4$ W $m^{-2}$ at 532 nm. (d) Local current−voltage data acquired at the three locations indicated in b and c. Inset: Local current−voltage data without illumination showing much smaller dark currents.

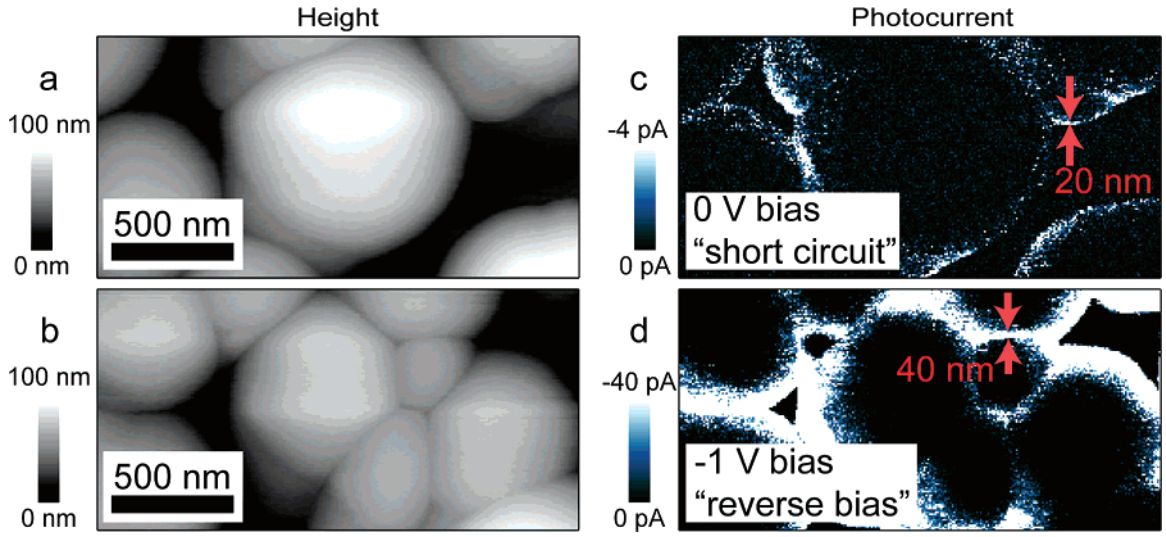


**Figure 2.** AFM height (a and b) and photocurrent (c and d) images taken of an MDMO-PPV:PCBM film spin-coated from toluene to give large phase separation. The active regions of the device show fwhm widths of ~20 nm for 0 V applied bias and ~40 nm for −1 V applied bias.

ORCA head model 59). Platinum-coated, contact-mode AFM tips were used, with manufacturer-specified tip diameters less than 25 nm (Budget Sensors, BS-ElectriCont). The height and current were measured simultaneously in contact mode. To measure photocurrents, a 5 mW, 532 nm laser, attenuated by neutral density filters, was focused onto the substrate and then aligned to the tip using the inverted optical microscope. More precise alignment and focusing was achieved by maximizing the photocurrent. Illumination intensities between ~10 and ~$10^8$ W $m^{-2}$ could be selected by a series of neutral density filters, including one continuously variable between optical density 0 and 4. The position and thus transmission through this filter was precisely controlled by a stepper motor.

Figure 1a shows a pcAFM image collected from an MDMO-PPV:PCBM film (20:80 spin-coated from xylenes). Significantly, this image was obtained at zero applied bias, demonstrating that we can obtain pcAFM images under short-circuit conditions. Furthermore, current−voltage data can be recorded at any location in the dark or under illumination. Parts b and c of Figure 1 plot the height and photocurrent at an illumination intensity of $10^4$ W $m^{-2}$. The photocurrent is lower in the MDMO-PPV-rich regions (low-topography regions[12−15]) and higher in the PCBM-rich regions (high-topography regions). Even among PCBM domains appearing similar in the topography image, a surprising range of photocurrents are observed. Photocurrent variations between topographically similar domains can be as large as a factor of 3. Figure 1d shows a series of current−voltage curves recorded at different points under illumination. The short-circuit current, the open-circuit voltage, and the fill factor are different for each domain, varying respectively from 1.4 to 26.4 pA, 0.35 to 0.53 V, and 0.42 to 0.58.

Photocurrent features as small as ~10 nm are visible in Figure 1c, suggesting a resolution similar to the AFM tip diameter when collected at zero bias. To confirm that the resolution is not significantly degraded by lateral charge transport, we have analyzed how such photocurrent maps evolve as the bias is changed. Figure 2 shows the topography, parts a and b, and photocurrent, parts c and d, measured from an MDMO-PPV:PCBM 20:80 film intentionally processed to exhibit very large domains (this MDMO-PPV was purchased from Aldrich, and the film was spin-coated from toluene, yielding a device with very low performance, but one that is useful for characterizing the technique). We see that charge is collected most efficiently at the domain interfaces. With a 0 V bias, Figure 2c, the fwhm width of these interfacial regions can be as small as 20 nm. With a −1 V bias, Figure 2d, the fwhm width of these active regions grows, but reaches only ~40 nm. It appears that even with a moderate applied bias, the resolution is still comparable with the tip diameter, however, the best resolution is obtained under short-circuit conditions.

By characterizing the same films in operating devices and with pcAFM, we find that the average photocurrent measured with the Pt tip agrees well with the photocurrents measured for bulk devices with Al contacts. Figure 3a compares two 1.5 $mm^2$ area devices with MDMO-PPV:PCBM 20:80 active layers spin-coated from chlorobenzene and xylenes. Chlorobenzene has previously been reported to be one of the best solvents for spin-coating efficient MDMO-PPV:PCBM solar cells.[11] Figure 3a compares the bulk EQEs measured at 532 nm monochromatic illumination (10 W $m^{-2}$) with the pcAFM photocurrents averaged over 2 $\mu$m × 2 $\mu$m areas (i.e., averaged over hundreds of polymer and PCBM domains, measured at $10^4$ W $m^{-2}$). The relative agreement is good, showing that the local photocurrents recorded by pcAFM provide information that is relevant to device performance. We have compared many films using both pcAFM and bulk device measurements (Supporting Information). In general, we find good qualitative agreement between the local pcAFM measurements and 1.5 $mm^2$ sized devices. However, the pcAFM measurements tend to yield slightly higher relative photocurrents for devices with high PCBM concentrations. We hypothesize that this difference could result from the different contact materials (Al top contacts versus Pt-coated

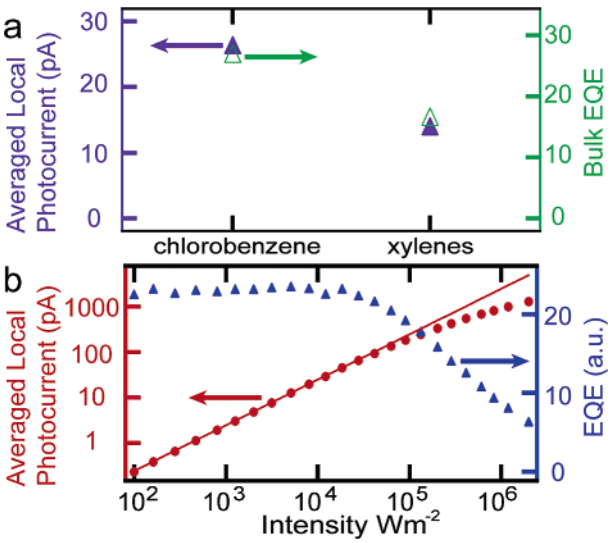


**Figure 3.** (a) The EQEs measured for bulk, MDMO-PPV:PCBM 20:80 devices (open triangles) are overlaid with the photocurrent averaged over $2 \times 2\ \mu m^2$ photocurrent images (filled triangles). (b) The photocurrent (red circles) at zero bias was measured as a function of light intensity in an MDMO-PPV:PCBM 20:80 film spin-coated from chlorobenzene (averaged over many locations); a linear fit is shown (solid red line). The relative EQE, determined by dividing the photocurrent by the intensity (blue triangles), is constant at intensities up to $5 \times 10^4$ W m$^{-2}$.

AFM tips) or the fact that the small fringe field in pcAFM leads to a slight double-counting of the more efficient domains.

Having demonstrated the ability to image photocurrents with high resolution, we next examine the intensity dependence of the photocurrent before turning to an analysis of the local photocurrent variations observed in Figures 1 and 2. One advantage of using a focused laser as an excitation source is that devices can be characterized over an extremely large range of illumination intensity. This ability is demonstrated in Figure 3b, which plots the photocurrent as a function of intensity for an MDMO-PPV:PCBM 20:80 film spin-coated from chlorobenzene. The intensity dependence is acquired by rotating the continuously variable neutral density filter and averaging over many locations. At low power, the photocurrent is seen to be nearly linearly proportional to illumination intensity, consistent with the reported intensity dependence of bulk devices,[40,41] and remains linear up to ~40 times solar intensity (Figure 3b). Because all the other photocurrent data presented in this paper were acquired at ~10 times solar intensity or lower (linear regime), the data in Figure 3b indicate that these pcAFM measurements are representative of performance at normal operating conditions. At intensities higher than ~40 times solar intensity, the intensity dependence becomes sublinear and suggestive of bimolecular recombination[40,41] or space-charge-limited photocurrent.[42] Although we do not explore this regime here, we believe that this ability to reach such intensities will prove valuable in future studies, perhaps using space-charge-limited photocurrent[42] to determine the ratio of electron to hole mobility at individual points in the film.

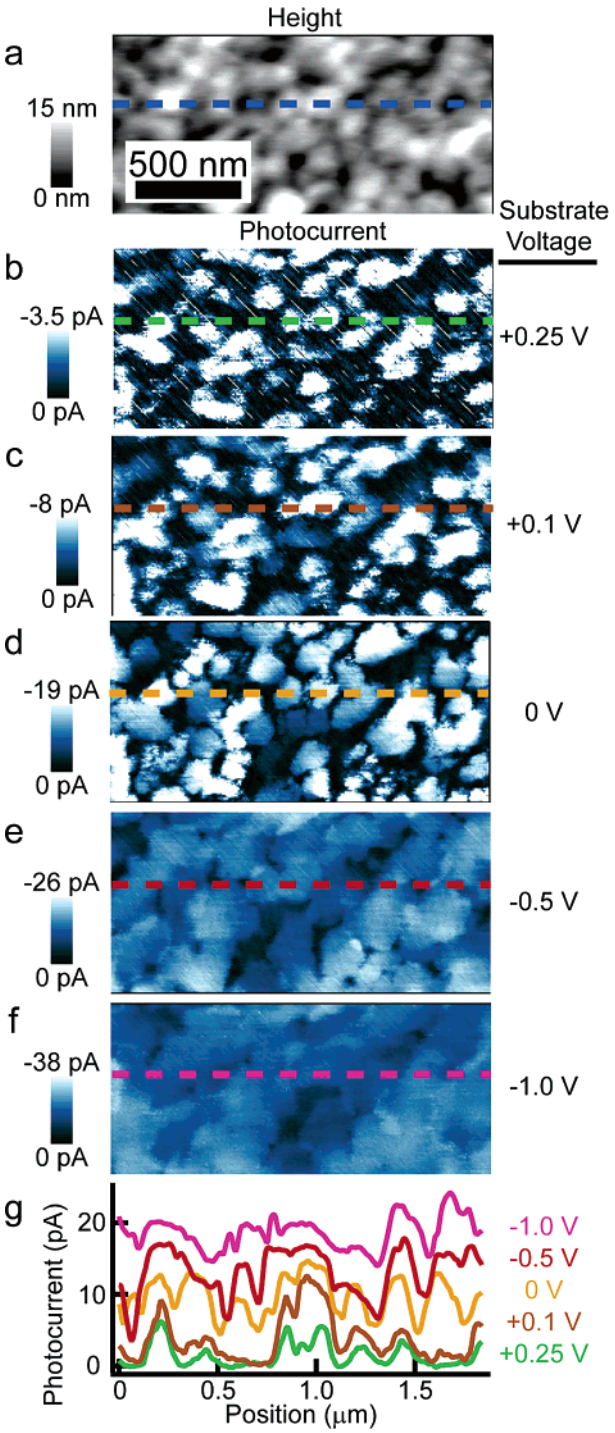


**Figure 4.** (a) AFM height image of an MDMO-PPV:PCBM 20:80 film spin-coated from xylenes. (b−f) Photocurrent images taken with applied biases between +0.25 V and −1.0 V, with an intensity of $10^4$ W m$^{-2}$. (g) Photocurrent line traces as indicated in b−f.

Beyond acquiring photocurrent images at zero bias, local performance can be methodically characterized between short-circuit and open-circuit conditions. Figure 4 presents such data for an MDMO-PPV:PCBM blend spin-coated from xylenes. Starting with a photocurrent image acquired with a bias of +0.25 V (near the open-circuit voltage), only a small fraction of the film generates current (Figure 4b). As the applied voltage becomes more negative, charge is collected more efficiently from all domains: the domains active at

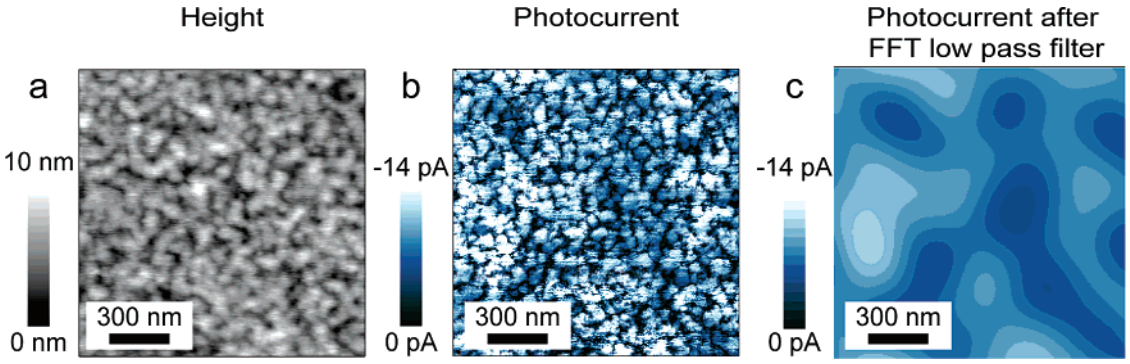


**Figure 5.** (a) AFM height image of an MDMO-PPV:PCBM 20:80 film spin-coated from chlorobenzene. (b) Photocurrent image taken with zero applied bias at an intensity of $5 \times 10^3$ W m$^{-2}$, and (c) processed with a 300 nm low-pass Fourier filter to emphasize the larger-scale variations in photocurrent.

zero bias produce more photocurrent, and additional regions of the film "turn on" and begin producing current. By −0.5 V (Figure 4e), nearly all of the film is generating high current, including most of the MDMO-PPV-rich region. By −1.0 V (Figure 4f), some MDMO-PPV-rich regions are producing even more current than the previously better PCBM domains, consistent with the higher electric fields, finally enabling collection of the charge in these optically dense regions. These trends can be visualized clearly in photocurrent line traces taken at each voltage (Figure 4g). This progression of individual domains "turning on" at different voltages indicates that the short-circuit current, open-circuit voltage, and fill factor are different for each domain (as can also be seen explicitly in Figure 1d). These local variations have important implications for bulk device efficiency. First, a device's short-circuit current could presumably be increased by fabricating a film where the entire area performed as well as the best "on" domains visible in Figure 4b. Second, a device's open-circuit voltage will be dominated by the open-circuit voltage of the best domains. Finally, a device's fill factor will be particularly dependent on microscopic variations; although it will not be better than the fill factor of the best domains, it will be reduced by those domains possessing low open-circuit voltages.

To quantify the importance of these spatial performance variations in the most efficient devices, we have mapped the short-circuit current of an MDMO-PPV:PCBM 20:80 film spin-coated from chlorobenzene (Figure 5). This gives smaller phase separation and better device performance[11] for this film: 42% EQE at 450 nm, a value within the typical literature range for devices with aluminum top contacts.[11−13,29] Despite the smaller phase separation produced by processing from chlorobenzene, the spatial variation in performance is still significant. The standard deviation of photocurrents in Figure 5b is ∼ 57% of the average value. The most efficient domains generate photocurrent ∼1.9 times higher than the average, suggesting that if the entire film was performing similarly, an EQE of ∼80% would be possible. Figure 5b also shows that, in addition to the variation between the individual ∼50 nm domains, the photocurrent also varies on a ∼200−600 nm length scale. This second, larger length scale of photocurrent variation can be more easily visualized by applying a low-pass Fourier filter to the photocurrent

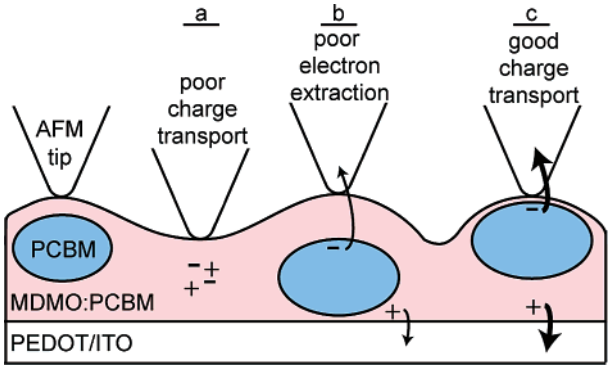


**Figure 6.** Proposed schematic of observed photocurrent variations. (a) MDMO-PPV-rich regions generate low photocurrents because of poor charge mobility and/or energy level alignment. (b) PCBM-rich regions generate more photocurrent, but the vertical position of a PCBM-rich domain and domain stacking can limit electron extraction, or (c) enhance electron extraction depending on the thickness of the MDMO-PPV:PCBM overlayer.

image (Figure 5c). The standard deviation of the photocurrent in Figure 5c is 15% of the average value, indicating that these larger features are still significant but of lesser importance than the individual domain variations.

Figure 6 outlines our hypothesis as to how domains that appear almost identical in AFM topography can appear so different in photocurrent images. We rule out local variations in film absorption based on experiments at various excitation wavelengths (Supporting Information). Instead, we propose that the variations result from differences in charge transport due to changes in vertical film structure. Extensive studies by others have shown that the morphology of a 20:80 MDMO-PPV:PCBM film consists of nearly pure PCBM domains encased in a matrix of ∼50:50 MDMO-PPV:PCBM material, such that, even in PCBM-rich regions, the polymer-rich shell surrounding each PCBM domain accounts for ∼35% of the device thickness.[12−15] Such a morphology ensures excellent charge generation, as can be confirmed by rapid photoluminescence quenching,[12] but does not always provide connected pathways for spatially uniform charge transport.

Indeed, cross-sectional TEM and SEM images of such films show both the stacking of multiple PCBM domains and variation in the vertical position of the PCBM domains

within the MDMO-PPV matrix.[14,22] Such vertical morphology will alter the efficiency of charge transport and extraction (Figure 6b,c). A related effect has already been observed in SKPM studies showing that changes in the polymer overlayer can alter the local open-circuit voltage.[22,23] We propose that similar variations in the MDMO-PPV overlayer modify charge transport and the tip−sample barrier height for charge extraction, thereby causing the variations in photocurrent and fill factor that we observe (Figure 6). We note that this hypothesis is consistent with the strong bias dependence of the variation; under increasing reverse bias, the applied field assists carrier extraction from the less-optimal morphologies (Figure 4g) until eventually all of the domains are "turned on".

While variations in vertical film structure can explain the differences in photocurrent between individual domains, Figure 5c also shows variations that occur on larger length scales and encompass multiple domains. These larger variations could potentially result from gradual larger-scale fluctuations in the MDMO-PPV overlayer thickness. However, these larger-scale photocurrent variations appear completely decoupled from the AFM topography. Furthermore, we observe nearly identical slowly varying photocurrent features in films spin-coated from xylenes, suggesting to us that these larger-length-scale fluctuations may not be associated with the MDMO-PPV:PCBM layer at all. We hypothesize that these larger features may instead be correlated with heterogeneities in the underlying ITO or PEDOT:PSS layers.[34,35,43] Verifying this hypothesis will require more detailed electrical imaging of the ITO and PEDOT:PSS films.

In conclusion, we have shown that pcAFM can be used to map photocurrents with ∼20 nm resolution and that these local photocurrents correlate with device performance. By applying pcAFM to image photocurrents in MDMO-PPV:PCBM blends, we have shown that the photocurrent is heterogeneous on two length scales. First, there are large variations in photocurrent between individual domains that we attribute to variations in vertical film structure. Second, there exist larger ∼200−600 nm scale fluctuations of unknown origin, possibly linked to the ITO or PEDOT:PSS layers. These heterogeneities in performance are visible even for films cast from chlorobenzene. On the basis of these observations, we conclude that local heterogeneity diminishes the fill factor and short-circuit current of even the current-best MDMO-PPV:PCBM devices. These results confirm that device performance can be improved by obtaining greater control and regularity of film morphology in both the lateral and vertical directions, and suggest that more work may be needed to characterize the buried ITO and PEDOT:PSS interfaces. Although we have used this technique to study MDMO-PPV:PCBM blends, its simplicity should allow for the characterization of many other organic blends over a wide range of illumination intensity. Further, as this technique is based on standard current−voltage measurements, albeit on solar cells the size of the AFM tip, it is interesting to speculate that other current−voltage based characterizations, including space-charge limited photocurrent and time-of-flight mobility measurements, might be accessible with high resolution.

**Acknowledgment.** This material is based on work supported by the National Science Foundation (DMR 0449422) and the STC Program of the National Science Foundation (DMR 0120967). D.S.G. is a Cottrell Scholar of the Research Corporation

**Supporting Information Available:** Additional experimental details, photocurrent images acquired with different wavelength illumination, and data comparing pcAFM photocurrent and device efficiency for MDMO-PPV:PCBM blends of various blend ratios. This material is available free of charge via the Internet at http://pubs.acs.org.

## References

(1) Shaheen, S. E.; Ginley, D. S.; Jabbour, G. E., *Mater. Res. Soc. Bull.* **2005**, *30*, 10.
(2) Nelson, J. *Science* **2001**, *293*, 1059.
(3) Koster, L. J. A.; Mihailetchi, V. D.; Blom, P. W. M. *Appl. Phys. Lett.* **2006**, *88*, 093511.
(4) Coakley, K. M.; McGehee, M. D. *Chem. Mater.* **2004**, *16*, 4533.
(5) Gregg, B. A. *Mater. Res. Soc. Bull.* **2005**, *30*, 20.
(6) Hoppe, H.; Sariciftci, N. S., *Mater. Res. Soc. Bull.* **2004**, *19*, 1924.
(7) Halls, J. J. M.; Walsh, C. A.; Greenham, N. C.; Marseglia, E. A.; Friend, R. H.; Moratti, S. C.; Holmes, A. B. *Nature* **1995**, *376*, 498.
(8) Yu, G.; Gao, J.; Hummelen, J. C.; Wudl, F.; Heeger, A. J. *Science* **1995**, *270*, 1789.
(9) Li, G.; Shrotriya, V.; Huang, J. S.; Yao, Y.; Moriarty, T.; Emery, K.; Yang, Y. *Nat. Mater.* **2005**, *4*, 864.
(10) Ma, W. L.; Yang, C. Y.; Gong, X.; Lee, K.; Heeger, A. J. *Adv. Funct. Mater.* **2005**, *15*, 1617.
(11) Shaheen, S. E.; Brabec, C. J.; Sariciftci, N. S.; Padinger, F.; Fromherz, T.; Hummelen, J. C. *Appl. Phys. Lett.* **2001**, *78*, 841.
(12) van Duren, J. K. J.; Yang, X. N.; Loos, J.; Bulle-Lieuwma, C. W. T.; Sieval, A. B.; Hummelen, J. C.; Janssen, R. A. J. *Adv. Funct. Mater.* **2004**, *14*, 425.
(13) Hoppe, H.; Glatzel, T.; Niggemann, M.; Schwinger, W.; Schaeffler, F.; Hinsch, A.; Lux-Steiner, M. C.; Sariciftci, N. S. *Thin Solid Films* **2006**, *511*, 587.
(14) Martens, T.; D'Haen, J.; Munters, T.; Beelen, Z.; Goris, L.; Manca, J.; D'Olieslaeger, M.; Vanderzande, D.; De Schepper, L.; Andriessen, R. *Synth. Met.* **2003**, *138*, 243.
(15) McNeill, C. R.; Watts, B.; Thomsen, L.; Belcher, W. J.; Kilcoyne, A. L. D.; Greenham, N. C.; Dastoor, P. C. *Small* **2006**, *2*, 1432.
(16) Chappell, J.; Lidzey, D. G.; Jukes, P. C.; Higgins, A. M.; Thompson, R. L.; O'Connor, S.; Grizzi, I.; Fletcher, R.; O'Brien, J.; Geoghegan, M.; Jones, R. A. L. *Nat. Mater.* **2003**, *2*, 616.
(17) McNeill, J. D.; Barbara, P. F. *J. Phys. Chem. B* **2002**, *106*, 4632.
(18) Cadby, A.; Dean, R.; Fox, A. M.; Jones, R. A. L.; Lidzey, D. G. *Nano Lett.* **2005**, *5*, 2232.
(19) Riehn, R.; Stevenson, R.; Richards, D.; Kang, D. J.; Blamire, M.; Downes, A.; Cacialli, F. *Adv. Funct. Mater.* **2006**, *16*, 469.
(20) McNeill, C. R.; Frohne, H.; Holdsworth, J. L.; Dastoor, P. C. *Nano Lett.* **2004**, *4*, 2503.
(21) DeAro, J. A.; Moses, D.; Buratto, S. K. *Appl. Phys. Lett.* **1999**, *75*, 3814.
(22) Hoppe, H.; Glatzel, T.; Niggemann, M.; Hinsch, A.; Lux-Steiner, M. C.; Saricifti, N. S. *Nano Lett.* **2005**, *5*, 269.
(23) Chiesa, M.; Burgi, L.; Kim, J. S.; Shikler, R.; Friend, R. H.; Sirringhaus, H. *Nano Lett.* **2005**, *5*, 559.
(24) Coffey, D. C.; Ginger, D. S. *Nat. Mater.* **2006**, *5*, 735.
(25) Chirvase, D.; Parisi, J.; Hummelen, J. C.; Dyakonov, V. *Nanotechnology* **2004**, *15*, 1317.
(26) Kim, Y.; Cook, S.; Tuladhar, S. M.; Choulis, S. A.; Nelson, J.; Durrant, J. R.; Bradley, D. D. C.; Giles, M.; McCulloch, I.; Ha, C. S.; Ree, M. *Nat. Mater.* **2006**, *5*, 197.
(27) Arias, A. C.; MacKenzie, J. D.; Stevenson, R.; Halls, J. J. M.; Inbasekaran, M.; Woo, E. P.; Richards, D.; Friend, R. H. *Macromolecules* **2001**, *34*, 6005.

(28) Coffey, D. C.; Ginger, D. S. *J. Am. Chem. Soc.* **2005**, *127*, 4564.
(29) Jeranko, T.; Tributsch, H.; Sariciftci, N. S.; Hummelen, J. C. *Sol. Energy Mater. Sol. Cells* **2004**, *83*, 247.
(30) Pingree, L. S. C.; Hersam, M. C.; Kern, M. M.; Scott, B. J.; Marks, T. J. *Appl. Phys. Lett.* **2004**, *85*, 344.
(31) Hersam, M. C.; Hoole, A. C. F.; O'Shea, S. J.; Welland, M. E. *Appl. Phys. Lett.* **1998**, *72*, 915.
(32) Paul, S.; Kanwal, A.; Chhowalla, M. *Nanotechnology* **2006**, *17*, 145.
(33) Lin, H. N.; Lin, H. L.; Wang, S. S.; Yu, L. S.; Perng, G. Y.; Chen, S. A.; Chen, S. H. *Appl. Phys. Lett.* **2002**, *81*, 2572.
(34) Liau, Y. H.; Scherer, N. F.; Rhodes, K. *J. Phys. Chem. B* **2001**, *105*, 3282.
(35) Ionescu-Zanetti, C.; Mechler, A.; Carter, S. A.; Lal, R. *Adv. Mater.* **2004**, *16*, 385.
(36) Alexeev, A.; Loos, J.; Koetse, M. M. *Ultramicroscopy* **2006**, *106*, 191.
(37) Douheret, O.; Lutsen, L.; Swinnen, A.; Breselge, M.; Vandewal, K.; Goris, L.; Manca, J. *Appl. Phys. Lett.* **2006**, *89*, 032107.
(38) Tuladhar, S. M.; Poplavsky, D.; Choulis, S. A.; Durrant, J. R.; Bradley, D. D. C.; Nelson, J. *Adv. Funct. Mater.* **2005**, *15*, 1171.
(39) Becker, H.; Spreitzer, H.; Ibrom, K.; Kreuder, W. *Macromolecules* **1999**, *32*, 4925.
(40) Koster, L. J. A.; Mihailetchi, V. D.; Blom, P. W. M. *Appl. Phys. Lett.* **2006**, *88*, 052104.
(41) Koster, L. J. A.; Mihailetchi, V. D.; Xie, H.; Blom, P. W. M. *Appl. Phys. Lett.* **2005**, *87*, 203502.
(42) Mihailetchi, V. D.; Wildeman, J.; Blom, P. W. M. *Phys. Rev. Lett.* **2005**, *94*, 126602.
(43) Armstrong, N. R.; Carter, C.; Donley, C.; Simmonds, A.; Lee, P.; Brumbach, M.; Kippelen, B.; Domercq, B.; Yoo, S. Y. *Thin Solid Films* **2003**, *445*, 342.

NL062989E